Preparation and room temperature NO_2-sensing performances of porous silicon/V_2O_5 nanorods*

Wen-Jun Yan(闫文君), Ming Hu(胡明), Ji-Ran Liang(梁继然),
Deng-Feng Wang(王登峰), Yu-Long Wei(魏玉龙), and Yu-Xiang Qin(秦玉香)†

School of Electronics and Information Engineering, Tianjin University, Tianjin 300072, *China*

(Received 21 October 2015; revised manuscript received 6 December 2015; published online 20 February 2016)

In this paper, porous silicon/V_2O_5 nanorod composites are prepared by a heating process of as-sputtered V film on porous silicon (PS) at 600 °C for different times (15, 30, and 45 min) in air. The morphologies and crystal structures of the samples are investigated by field emission scanning electron microscope (FESEM), x-ray diffractometer (XRD), x-ray photoelectron spectroscopy (XPS), and Raman spectrum (RS). An improved understanding of the growth process of V_2O_5 nanorods on PS is presented. The gas sensing properties of samples are measured for NO_2 gas of 0.25 ppm∼3 ppm at 25 °C. We investigate the effects of the annealing time on the NO_2-sensing performances of the samples. The sample obtained at 600 °C for 30 min exhibits a very strong response and fast response-recovery rate to ppm level NO_2, indicating a p-type semiconducting behavior. The XPS analysis reveals that the heating process for 30 min produces the biggest number of oxygen vacancies in the nanorods, which is highly beneficial to gas sensing. The significant NO_2 sensing performance of the sample obtained at 600 °C for 30 min probably is due to the strong amplification effect of the heterojunction between PS and V_2O_5 and a large number of oxygen vacancies in the nanorods.

Keywords: V_2O_5 nanorods, porous silicon, heterojunction, NO_2-sensing

PACS: 07.07.Df, 81.07.–b, 68.35.bg, 68.65.–k **DOI:** 10.1088/1674-1056/25/4/040702

1. Introduction

Today, NO_2 sensor is the need of the hour that could have high sensitivity and low operating temperature at low concentrations. Solid-state resistive-type gas sensors based on one-dimensional metal oxide semiconductors (1D MOS) with large surface-to-volume ratios, have been widely used for sensing NO_2 gas.[1–4] Despite the promising potential of 1D MOS for NO_2 gas sensor applications, some aspects such as improvement of sensitivity, low selectivity and high operating temperature are persistent challenges to their actual implementation. Many recent studies have shown that the important sensing parameters of 1D MOS sensors can be improved by making the composite with others,[5] e.g., noble metals,[6–8] dissimilar metal oxides,[9–14] organics,[15] and other semiconductors.[16–19]

As two kinds of important semiconductors, V_2O_5 and porous silicon (PS) have gained more and more attention over the past decade.[20–22] V_2O_5 offers the possibility to be a reliable sensing material due to its layered crystal structure. To date, 1D V_2O_5 nanostructures have been used for detecting gases such as ethanol[23,24] and ammonia.[25,26] However, there are rare reports about V_2O_5 based NO_2 sensors. Yu *et al.*[27] reported V_2O_5 nanotubes response to both ethanol vapor and NO_2 gases at 80 °C. This sensor has two shortcomings including poor selectivity between gases and relatively high operating temperature (e.g. 80 °C).

PS has been used extensively for detecting NO_2 at low temperatures due to its large specific surface area and high chemical reactivity.[20,28] However, the instability of gas-sensitivity and lack of thermal stability restrict the commercial applications of PS. A gas sensor based on composites of PS and low-dimensional nanomaterials may be beneficial for enhancing gas response properties for their synergetic enhancement or heterojunction effects. There are rare reports about the gas sensing properties of PS and metal oxide nanostructures (ZnO, WO_3, etc.).[29–31] The special composites exhibit a significant improvement on gas sensing performances with respect to the monocomponent, therefore the heterojunction barrier-controlled sensing mechanism is proposed. In our previous work, the high sensitivity and selectivity of the PS/V_2O_5 nanorods to NO_2 gas at room temperature were reported, but no detailed study on the growth mechanism of the nanorods on PS nor the effect of the synthesis process on its NO_2-sensing performance was conducted.

In the present work, the PS/V_2O_5 composite is prepared by a very simple non-catalytic one-step process of directly annealing PS/V film. We describe the growth process of the V_2O_5 nanorods synthesized from V film on the PS substrate. The effects of heat treatment on the microstructure and gas sensing properties of the samples are investigated. Field emission scanning electron microscope (FESEM) is used to study the surface morphology. The crystalline properties and phases are determined by an x-ray diffractometer (XRD) and Raman

*Project supported by the National Natural Science Foundation of China (Grant Nos. 61271070, 61274074, and 61574100).
†Corresponding author. E-mail: qinyuxiang@tju.edu.cn
© 2016 Chinese Physical Society and IOP Publishing Ltd

analysis. X-ray photoelectron spectroscopy (XPS) is used to determine the chemical composition of the samples.

2. Experiment

PS was prepared by the galvanostatic electrochemical etching of p-type monocrystalline silicon (100) wafer (resistivity 10 Ω·cm–15 Ω·cm). The electrolyte was a mixture of 40 wt% HF and 99.5 wt% N, N-dimethyl formamide with 1:2 volume ratio. The anodization was performed for 8 min with an etching current density of 100 mA/cm^2 as described in our previous work.[32] The average pore size of the obtained PS is $\sim$ 1.2 μm in diameter and 12 μm in depth. The porosity of the porous layer is 39%–42%.

The V_2O_5 nanorods on PS were prepared through magnetron sputtering followed by annealing as described in our previous work.[33] Firstly, a V film with a thickness of $\sim$ 300 nm was deposited on PS by DC magnetron sputtering. The sputtering conditions were as follows: 2 mm in diameter, 3-mm thick V target (purity 99.999%); input power of 135 W; chamber atmosphere of 2-Pa Ar; deposition carried out for 40 min. The V-deposited PSs were subsequently annealed in air at 300, 400, 500, and 600 °C for different times (15, 30, and 45 min) in a standard program-controlled furnace with a heating rate of 5 °C/min. After the annealing process, the samples were cooled down inside the furnace to make the V_2O_5 nanorods suitably crystallized and stabilized. As a result, different V_2O_5 nanostructures were obtained on PSs.

The different V_2O_5 nanostructures formed on PSs were analyzed by using various characterization techniques. FE-SEM (FEI Nanosem 430) and transmission electron microscopy (TEM, Tecnai G2 F20) were employed to examine microstructures. XRD (D/MAX 2500) with Cu Kα radiation was used to investigate the phases and crystalline structures of samples. XPS (Perkin elemer PHI-1600 ESCA System) with a Mg K$_\alpha$ excitation source was used to characterize the surface elemental composition distribution profile and chemical state. Raman spectrum (RS) (Thermo Scientific confocal DXR Raman microscope) with a 532-nm wavelength Nd:YAG laser was used to characterize the bond configuration.

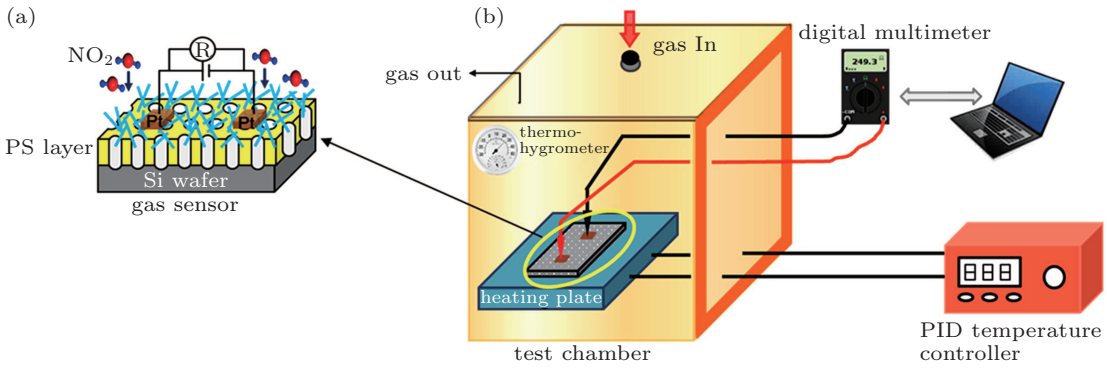


Fig. 1. (color online) Schematic diagram of (a) the resistive-type nanocomposite gas sensor and (b) the gas sensing measurement system.

The gas sensing properties of PS/V_2O_5 composites were evaluated in a static gas sensing characterization system consisting of a glass test chamber, a flat heating plate, a programmable digital multimeter and data acquisition system.[34] In order to realize the electrically ohmic connection between the sensor and the digital multimeter, two $\sim$ 120-nm-thick Pt film electrodes were deposited onto the surface of the PS/V_2O_5 composite by magnetron sputtering. Figures 1(a) and 1(b) show the schematic diagrams of the resistive-type gas sensor and the gas sensing test system respectively. In the whole measuring process, NO_2 gas was introduced into the chamber directly to obtain the desired concentration, and the ambient relative humidity was about 30% which was controlled by using a dehumidifier. The sensitivity was defined as R_a/R_g, where R_a and R_g are the electrical resistances in air and in NO_2 gas, respectively.

3. Results and discussion

3.1. Structure characterizations

Figure 2 shows the XRD patterns of different V_2O_5 nanostructures on PS synthesized in air atmosphere for 30 min in a temperature range of 300 °C–600 °C. The absence of obvious diffraction peaks demonstrates that the 300 °C–400 °C annealed sample has an amorphous structure. It indicates that the heating treatment of V film below 400 °C in air did not induce significant crystallinity. Only small peaks appear even for the sample heat-treated at a temperature of 500 °C, indicating significant crystallinity in the structure of PS/V_2O_5, whereas after heat-treatment at 600 °C in air, the sample has a sharp diffraction peak. All recognizable diffraction peaks, obtained at $2\theta = 15.484°$, $20.412°$, $21.847°$, $26.315°$, $31.197°$, $41.443°$, can be well indexed to an orthorhombic V_2O_5 phase with a lattice parameter of $a = 11.48$ Å, $b = 4.36$ Å, $c = 3.55$ Å

(JCPDS:72-0598). The strongest sharp peak appears at $2\theta = 20.39°$, corresponding to the V_2O_5 (010).

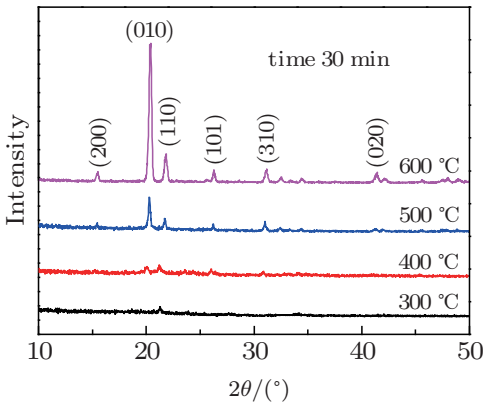


Fig. 2. (color online) XRD patterns of V_2O_5 products on PS synthesized at different temperatures for 30 min.

Figures 3(a)–3(d) show the SEM images of the as-prepared V film with 300 nm in thickness on the PS surface, and the samples annealed at 400, 500, and 600 °C for 30 min in air atmosphere respectively. It is clear that the surface morphologies mainly depend on the annealing temperature just as indicated in other reports.[35,36] The as-deposited V film shows a continuous surface with small grain size on the surface of the PS skeleton, while the grain size of V_2O_5 nanostructures increases with the increase of annealing temperature. Remarkably, only particles were produced at 400 °C; with a temperature increase, both the number of particles and the sizes of the particles increase, and nearly layered crystal particles appear at 500 °C; at a temperature of 600 °C, long striped V_2O_5 nanorods with a typical size of about 6 μm×0.1 μm×0.04 μm were synthesized on the PS surface (Fig. 3(d)).

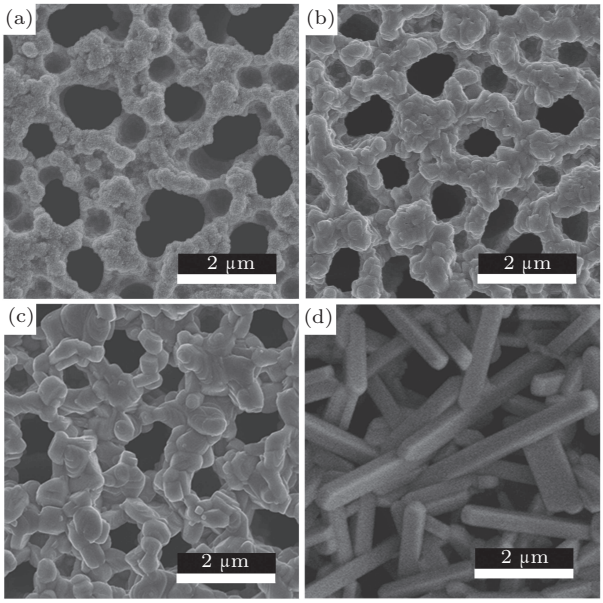


Fig. 3. SEM images of (a) the as-deposited V film with 300 nm in thickness on the PS surface, and annealed samples for 30 min at (b) 400 °C, (c) 500 °C, and (d) 600 °C respectively.

In order to investigate the synthesis process of the V_2O_5 nanorods on PS deeply, we anneal the as-deposited V film on PS at 600 °C for different times (15, 30, and 45 min) in air atmosphere. The surface morphologies and XRD patterns of the samples annealed at 600 °C for different times are shown in Figs. 4(a)–4(c). As shown in Figs. 4(a), 4(b), and 3(d), for different heat-treated times (15 min–45 min), V_2O_5 nanorods show slight modifications in size and quantity. Figure 4(c) shows the XRD patterns of V_2O_5 nanorods formed on the PS at 600 °C for different times. All the recognizable diffraction peaks of the PS/V_2O_5 prepared at 600 °C for 15, 30, and 45 min agree with those of an orthorhombic V_2O_5 listed in JCPDS card No. 72-0598. Yet, the XRD intensity of PS/V_2O_5 prepared at 600 °C for 15 min is weaker than those for 30 min and 45 min. The XRD intensity of V_2O_5 is almost unchanged by increasing the heat-treated time (> 30 min).

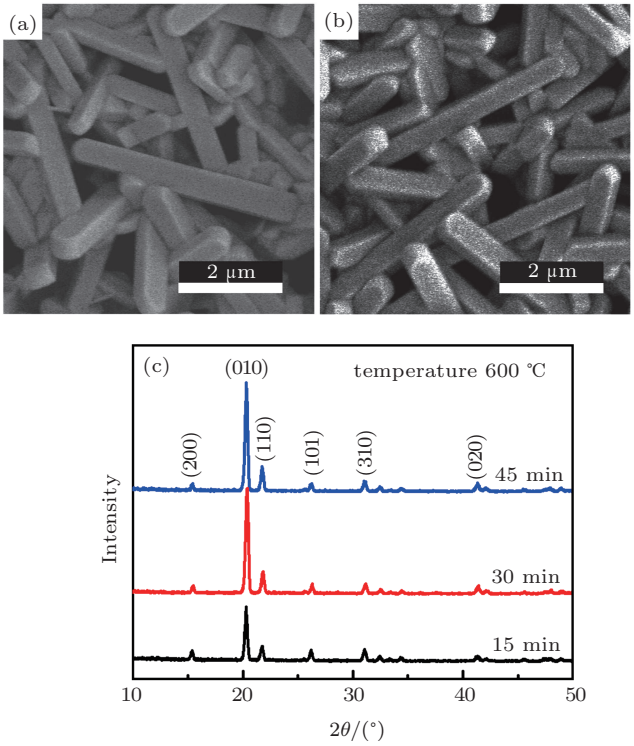


Fig. 4. (color online) SEM images of PS/V_2O_5 nanorods annealed at 600 °C for (a) 15 min and (b) 45 min. (c) XRD patterns of V_2O_5 nanorods synthesized at 600 °C for different times.

The microstructures of V_2O_5 nanorods annealed at 600 °C are further confirmed using XPS. Figures 5(a)–5(c) show the high resolution core level V 2p spectra. The literature reported binding energy (E_b) for V $2p_{3/2}$ is (517 ± 0.3) eV.[37] The observed values of 517.04, 517.15, and 517.12 eV for the samples annealed for 15, 30, and, 45 min respectively agree well with those of V^{5+} in V_2O_5. It is noteworthy that the sample annealed for 30 min shifts the V $2p_{3/2}$ peak up to 517.15 eV. This can be explained by considering the fact that if an oxygen vacancy exists in the nanorods, the electronic

density near its adjacent V atom decreases, which raises the V $2p_{3/2}$ level banding energy. It can be concluded that more oxygen vacancies exist in the sample annealed for 30 min than in the samples annealed for 15 min and 45 min. This indicates that oxygen vacancies exist in the V_2O_5 nanorods; what is more, more oxygen vacancies remain in the sample annealed for 30 min than the samples annealed for 15 min and 45 min. Oxygen vacancies play an important role as adsorption sites for gaseous species and eventually a minor shift of the E_b may imply greatly enhanced gas sensitivity.[38]

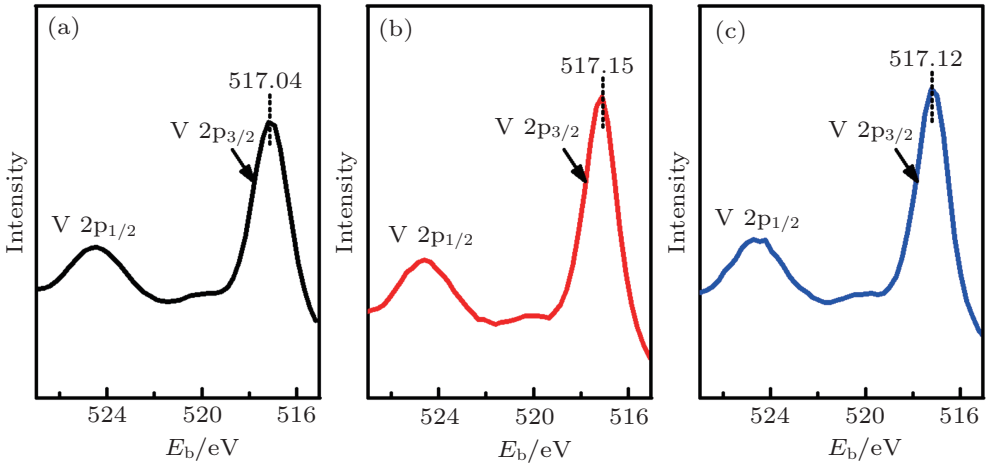


Fig. 5. (color online) High resolution XPS core level V 2p spectra of PS/V_2O_5 nanorods annealed at 600 °C for (a) 15 min, (b) 30 min, and (c) 45 min.

To further investigate the microstructure of PS/V_2O_5 nanorods at 600 °C for 30 min, the RS is measured, which is shown in Fig. 6. The sharp peak at 516.23 cm^{-1} belongs to the PS substrate. Those peaks located at 140.45, 279.80, 698.25, and 990.55 cm^{-1}, can be indexed to the Raman signature of the V_2O_5 crystal.[39] The predominant low-wavenumber band at 140.45 cm^{-1} is attributed to the skeleton bent vibration, and the peak at 279.80 cm^{-1} is from the bending vibrations of the O_C–V–O_B bond. The stretching vibration of the V–O_C bond occurs at about 698.25 cm^{-1}. The layered structure of V_2O_5 is stacked up from the distorted trigonal bipyramidal coordination polyhedron of oxygen atoms around vanadium atoms.[40] The mode of the skeleton bent, corresponding to the peak at 140.45 cm^{-1}, is the evidence for the layered structure of V_2O_5 nanorods. Furthermore, the peak at 990.55 cm^{-1}, corresponding to the stretching of the V=O bond, is also a significant clue to the layer-type structure property of V_2O_5 nanorods.[40]

Through analyzing the morphological and structural characteristics of V_2O_5 nanorods grown on PS, we try to explain the growth mechanism of the nanorods. We suppose that the process of V_2O_5 nanorods is related to the surface morphology of the substrate PS and the annealing temperature. Boston *et al.*[41] indicated that sites on the rough surface of the porous matrix act as microcrucibles and thus provide an insight into the mechanism that drive metal oxide nanowire growth at high temperatures. According to the result of Zou *et al.*,[36] after annealing in oxygen ambience, the as-sputtered amorphous V_2O_5 films on glass substrates dramatically transform into V_2O_5 nanorods and large V_2O_5 particles on Si substrate, because on the glass, the as-prepared V_2O_5 shows a textured surface, while the as-prepared film on Si is much smoother.

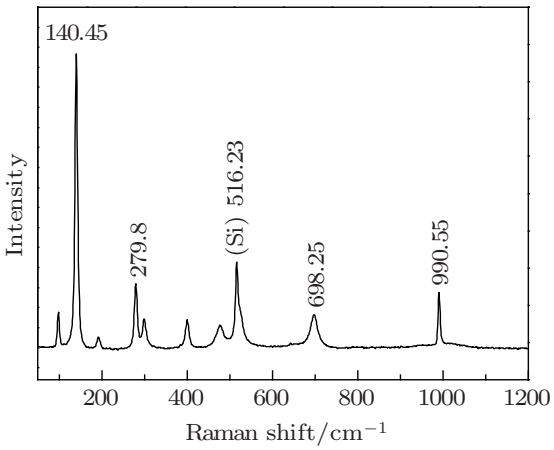


Fig. 6. Raman spectrum of PS/V_2O_5 nanorods annealed at 600 °C for 30 min.

Here, V granular film deposited on PS reacts with O_2 in air ambience with furnace temperature increasing. But the post annealing treatment below 400 °C does not provide enough energy to form a crystal structure, resulting in the amorphous V_2O_5. The next crystallization process of amorphous V_2O_5 is sensitive to the temperature in a range from 400 °C to 500 °C. Furthermore, the rough surface of the substrate PS can act as the nucleation site to benefit the growth of V_2O_5 nanorods, and the thermodynamic-related surface diffusion controls the process at high temperatures. Ultimately, the initial V film transforms into V_2O_5 nanorods completely after annealing at 600 °C. The crystallization process is illustrated in Fig. 7.

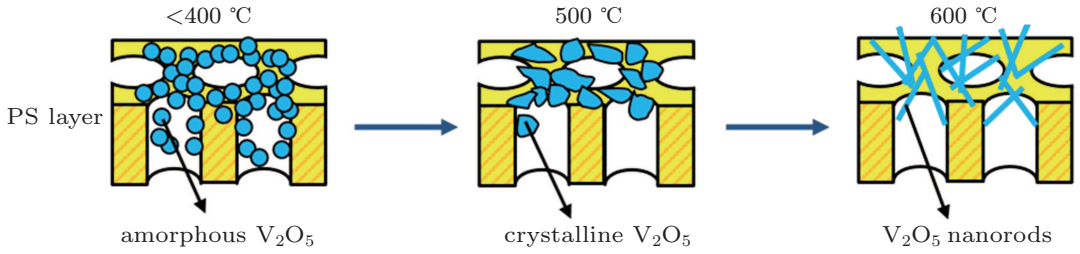


Fig. 7. (color online) Schematic drawing of the formation process of V_2O_5 nanorods.

3.2. NO_2-sensing performances

As reported in our previous work, the optimum operating temperature of PS/V_2O_5 nanorods is 25 °C.[33] Thus the subsequent gas sensing measurements are carried out at 25 °C.

Figure 8(a) shows the relationships between NO_2 concentration and sensitivity of PS/V_2O_5 nanorods synthesized at 600 °C for different times at room temperature. As shown in Fig. 8(a), all the sensitivity values (R_a/R_g) are larger than 1 at 25 °C, which implies that the PS/V_2O_5 nanorods indicate a typical p-type semiconductor behavior to NO_2 gas. This phenomenon is attributed to the heterojunction between PS and V_2O_5, which has been discussed in our previous report.[33] What is more, the sample synthesized at 600 °C for 30 min exhibits a higher sensitivity than the others in the whole concentration range from 0.25 ppm to 3 ppm (according to Fig. 8(a)), which is mainly due to its improved properties in crystallinity and oxygen vacancies.

Figure 8(b) shows the dynamic responses of the sample synthesized at 600 °C for 30 min to NO_2 with different concentrations. As shown in Fig. 8(b), the resistance variation of the sample is strongly dependent on NO_2 concentration, and its lower limit of detection of NO_2 is 0.25 ppm with a sensitivity of 1.65, while its sensitivity to NO_2 of 3 ppm is 9.43. Resistance of the sample dramatically decreases upon exposure to NO_2 gas and completely returns to its original value after evacuating the unused gas from the chamber, indicating a p-type conductive property.

Furthermore, listed in Table 1 are the NO_2 gas responses of the PS/V_2O_5 nanorods sensor with those of other reported V_2O_5 sensors. It should be noted that the NO_2 concentration and the operating temperature used in the present study are lower than those in previous works but the response is higher than that of those gas sensors.

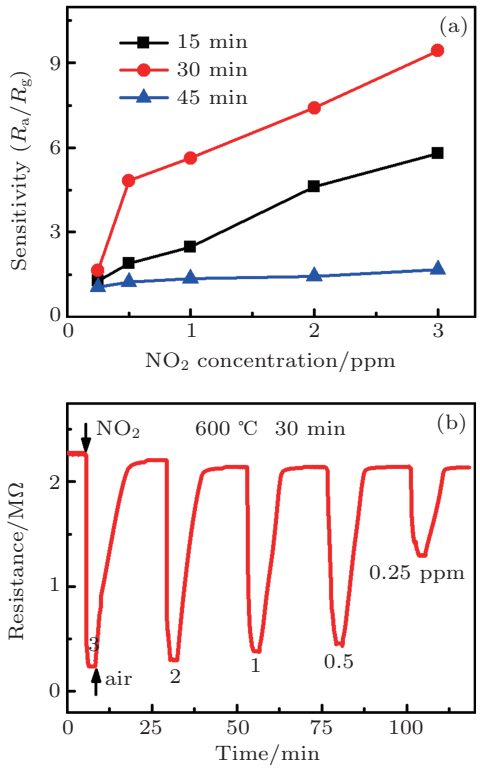


Fig. 8. (color online) (a) NO_2 concentration-dependent response values of PS/V_2O_5 nanorods at 25 °C. (b) Dynamic response curve of PS/V_2O_5 nanorods annealed at 600 °C for 30 min to various concentrations of NO_2 at 25 °C.

Table 1. Comparisons of the response, NO_2 testing concentration and operating temperature between the PS/V_2O_5 nanorods and other V_2O_5 sensors.

Nanomaterials	Response	NO_2 concentration/ppm	Temperature/°C	Ref.
V_2O_5 nanotubes	1.11	5	80	[27]
1D ZnO–V_2O_5	8	5	350	[42]
1D SnO_2/V_2O_5 core-shell	1.03	10	300	[43]
V_2O_5–WO_3 film	9	10	250	[44]
PS/V_2O_5 nanorods	9.43	3	RT	present

The response time and recovery time of the PS/V_2O_5 nanorods synthesized at 600 °C for 30 min each as a function of NO_2 concentration is shown in Fig. 9. It can be seen that the response time decreases from 96 s to 10 s, whereas the recovery time increases from 282 s to 474 s with NO_2 concentration increasing from 0.25 to 3 ppm, respectively. As expected, the

sensor shows a fast response characteristic, which is very important in the gas-sensing applications. Yet, the relatively long recovery time remains to be improved. Meanwhile, it is observed that the response time and recovery time vary inversely with target gas concentration. A higher NO_2 concentration implies that NO_2 gas molecules can diffuse more sufficiently in the test chamber and into the PS/V_2O_5 nanorods composite. Therefore, a shorter response time and a larger resistance change are achieved, while the weaker ability to desorb the large quantity of gas species results in a prolonged recovery time.

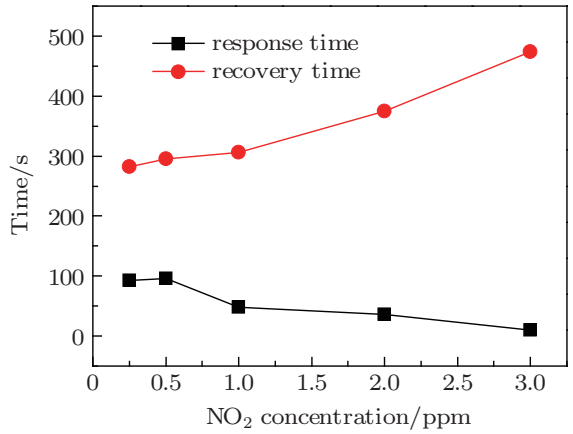


Fig. 9. (color online) Variations of response time and recovery time of the PS/V_2O_5 nanorods synthesized at 600 °C for 30 min with NO_2 concentration.

Since V_2O_5 behaves as an n-type semiconductor in gas sensing which is controlled by the surface conductance, the hetero-structure (p-PS/n-V_2O_5) is formed at the interface between them. In the hetero-structure, a depletion layer and the associated potential barrier exist. Both the PS and V_2O_5 nanorods can result in a specially large density of oxygen vacancy defects and dangling bonds, which makes the surface of the PS/V_2O_5 composite much more active in absorbing oxygen. The enhanced oxygen molecules adsorbed on the surface capture more free electrons from the conducting band. As a result, the depletion region is increased and the band bending is further, leading to an inversion layer instead of a depletion layer and indicating a p-type semiconductor property. As observed in XPS analysis, the sample synthesized at 600 °C for 30 min attains the maximal number of oxygen vacancies on the surface, leading to its greatest response to NO_2.

4. Conclusions

A composite of PS/V_2O_5 nanorods is fabricated by an efficient non-catalytic method based on heating sputtering-deposited pure V film on PS in air at 600 °C. The process of the V_2O_5 nanorods growth on PS is investigated. The rough surface of the substrate PS acts as the nucleation sites to benefit the growth of V_2O_5 nanorods, and the thermodynamic-related surface diffusion controls the process at high temperatures. Oxygen vacancies are introduced into the composite structure in the annealing process. All the samples indicate a p-type conductive sensing behavior to NO_2 gas at 25 °C. However, the sample annealed at 600 °C for 30 min shows the strongest response to ppm level NO_2 with a fast response-recovery rate, owing to its improved crystallinity and significant oxygen vacancies.

References

[1] Wang Y L, Jiang X C and Xia Y N 2003 *J. Am. Chem. Soc.* **125** 16176
[2] Kolmakov A and Moskovits M 2004 *Ann. Rev. Mater. Res.* **34** 151
[3] Li C, Zhang D H, Liu X L, Han S, Tang T, Han J and Zhou C W 2003 *Appl. Phys. Lett.* **82** 1613
[4] Li S, Li F L and Zhou S M 2009 *Chin. Phys. B* **18** 3985
[5] Miller D R, Akbar S A and Morris P A 2014 *Sens. Actuators B: Chem.* **204** 250
[6] Kolmakov A, Klenov D O, Lilach Y, Stemmer S and Moskovits M 2005 *Nano Lett.* **5** 667
[7] Li X W, Zhou X, Guo H, Wang C, Liu J Y, Sun P, Liu F M and Lu G Y 2014 *ACS Appl. Mater. Interfaces* **6** 18661
[8] Shin J, Choi S J, Lee I, Youn D Y, Park C O, Lee J H, Tuller H L and Kim I D 2013 *Adv. Funct. Mater.* **23** 2357
[9] Bai S L, Chen S, Zhao Y B, Guo T, Luo R X, Li D Q and Chen A F 2014 *J. Mater. Chem. A* **2** 16697
[10] Liu C B, He Y and Wang S L 2015 *Chin. Phys. B* **24** 118501
[11] Bai S, Guo T, Zhao Y, Luo R, Li D, Chen A and Liu C C 2013 *J. Mater. Chem. A* **1** 11335
[12] Huang H, Gong H, Chow C L, Guo J, White T J, Tse M S and Tan O K 2011 *Adv. Funct. Mater.* **21** 2680
[13] Mashock M, Yu K H, Cui S M, Mao S, Lu G H and Chen J H 2012 *ACS Appl. Mater. Interfaces* **4** 4192
[14] Park S, An S, Mun Y and Lee C 2013 *ACS Appl. Mater. Interfaces* **5** 4285
[15] Kim I D, Rothschild A, Lee B H, Kim D Y, Jo S M and Tuller H L 2006 *Nano Lett.* **6** 2009
[16] Wongchoosuk C, Wisitsoraat A, Phokharatkul D, Tuantranont A and Kerdcharoen T 2010 *Sensors* **10** 7705
[17] Yan D L, Hu M, Li S Y, Liang J R, Wu Y Q and Ma S Y 2014 *Electrochim. Acta* **115** 297
[18] An X Q, Yu J C, Wang Y, Hu Y M, Yu X L and Zhang G J 2012 *J. Mater. Chem.* **22** 8525
[19] Niu F, Liu J M, Tao L M, Wang W and Song W G 2013 *J. Mater. Chem. A* **1** 6130
[20] Ozdemir S and Gole J L 2007 *Curr. Opin. Solid St. Mater. Sci.* **11** 92
[21] Cao A M, Hu J S, Liang H P and Wan L J 2005 *Angew. Chem.-Int. Ed.* **44** 4391
[22] Gu G, Schmid M, Chiu P W, Minett A, Fraysse J, Kim G T, Roth S, Kozlov M, Munoz E and Baughman R H 2003 *Nat. Mater.* **2** 316
[23] Leroy C M, Achard M-F, Babot O, Steunou N, Massé P, Livage J, Binet L, Brun N and Backov R 2007 *Chem. Mater.* **19** 3988
[24] Jin W, Yan S L, An L, Chen W, Yang S, Zhao C X and Dai Y 2015 *Sens. Actuators B: Chem.* **206** 284
[25] Modafferi V, Panzera G, Donato A, Antonucci P L, Cannilla C, Donato N, Spadaro D and Neri G 2012 *Sens. Actuators B: Chem.* **163** 61
[26] Raible I, Burghard M, Schlecht U, Yasuda A and Vossmeyer T 2005 *Sens. Actuators B: Chem.* **106** 730
[27] Yu M L, Liu X Q, Wang Y, Zheng Y B, Zhang J W, Li M Y, Lan W and Su Q 2012 *Appl. Surf. Sci.* **258** 9554
[28] Li M D, Hu M, Liu Q L, Ma S Y and Sun P 2013 *Appl. Surf. Sci.* **268** 188

[29] Kanungo J, Saha H and Basu S 2010 *Sens. Actuators B: Chem.* **147** 128
[30] Kumar Y, Garcia J E, Singh F, Olive-Mendez S F, Sivakumar V V, Kanjilal D and Agarwal V 2012 *Appl. Surf. Sci.* **258** 2283
[31] Mendoza-Aguero N, Kumar Y, Olive-Mendez S F, Campos-Alvarez J and Agarwal V 2014 *Ceram. Int.* **40** 16603
[32] Yan W J, Hu M, Zeng P, Ma S Y and Li M D 2014 *Appl. Surf. Sci.* **292** 551
[33] Yan W, Hu M, Wang D and Li C 2015 *Appl. Surf. Sci.* **346** 216
[34] Li M D, Hu M, Yan W J, Ma S Y, Zeng P and Qin Y X 2013 *Electrochim. Acta* **113** 354
[35] Zou C W, Yan X D, Patterson D A, Emanuelsson E A C, Bian J M and Gao W 2010 *Crystengcomm* **12** 691
[36] Zou C W, Fan L L, Chen R Q, Yan X D, Yan W S, Pan G Q, Wu Z Y and Gao W 2012 *Crystengcomm* **14** 626
[37] Sathiya M, Prakash A S, Ramesha K, Tarascon J M and Shukla A K 2011 *J. Am. Chem. Soc.* **133** 16291
[38] Maffeis T G G, Yung D, LePennec L, Penny M W, Cobley R J, Comini E, Sberveglieri G and Wilks S P 2007 *Surf. Sci.* **601** 4953
[39] Su Q, Huang C K, Wang Y, Fan Y C, Lu B A, Lan W, Wang Y Y and Liu X Q 2009 *J. Alloys Compd.* **475** 518
[40] Chernova N A, Roppolo M, Dillon A C and Whittingham M S 2009 *J. Mater. Chem.* **19** 2526
[41] Boston R, Schnepp Z, Nemoto Y, Sakka Y and Hall S R 2014 *Science* **344** 623
[42] Liang Y C and Cheng Y R 2015 *Crystengcomm* **17** 5801
[43] Kim H S, Jin C H, Park S H and Lee C M 2013 *J. Electroceram.* **30** 6
[44] He X L, Li J P and Gao X G 2004 *Sens. Actuators B: Chem.* **108** 207